Proceedings World Geothermal Congress 2020+1
Reykjavik, Iceland, April - October 2021

Mapping Geothermal Vegetation with Hyperspectral and Thermal Imaging – A New Way to Explore Geothermal Areas

Rodriguez-Gomez C.[1], Kereszturi, G.[1], Reeves, R.[2], Rae, A.[2], Pullanagari, R.[3], Jeyakumar, P.[1], Procter, J.[1]

[1] Institute of Agriculture and Environment, Massey University, Palmerston North, New Zealand

[2] GNS Science, Wairakei Research Centre, Taupo, New Zealand

[3] MAF digital Lab, School of Food and Advanced Technology, Massey University, Palmerston North, New Zealand

c.gomez@massey.ac.nz

Keywords: Geothermal exploration, geothermal vegetation, hyperspectral remote sensing, thermal infrared remote sensing, New Zealand.

ABSTRACT

Vegetation can reflect activity of a geothermal system, through interactions between soil-chemical conditions, heat and gas emissions. Some plant species are extremely capable of thriving in such environments, such as kanuka (i.e. *kunzea ericoides* var. *microflora*), an endemic shrub of geothermal areas in the Taupo Volcanic Zone (TVZ), New Zealand. Remote sensing studies have targeted vegetation vigour on active geothermal areas, which can provide a fast and cheap surface exploration method as well as monitoring. In this study, airborne hyperspectral and thermal data has been acquired over the Waiotapu Geothermal Field, New Zealand to detect spatial distributions of kanuka, selected from a supervised classification. To the areas detected as kanuka a variety of vegetation indices (including Normalised Difference Vegetation Index, Simple Ratio Index, Red Edge Normalised Difference Vegetation Index, Vogelmann Index) were applied giving an insight to the overall health of kanuka in the Waiotapu Geothermal Field. The vegetation indices and the thermal infrared image spatial distributions were analysed by visual interpretation and quantitative analysis. This combined methodology allows to interpret the correlations that the kanuka plant has with geothermal heat flux, and therefore a path to utilise kanuka shrub as a proxy to detect active geothermal systems from a remote sensing platform.

1. INTRODUCTION

Geothermal exploration incorporates a variety of geological techniques (Mauriohooho et al., 2014; Simpson and Rae, 2018; Wilson et al., 1995), geophysical techniques (Bibby et al., 1994; Calvin et al., 2005; Hochstein and Soengkono, 1997; Mongillo, 1994; Reeves and Rae, 2016) and geochemical techniques (Blasco et al., 2018; Bobos and Williams, 2017; Burgos, 1999) with the main purpose of characterising the subsurface hydrogeological system. Geothermal areas formed by circulation of hydrothermal fluids in the subsurface through fractured and permeable rocks, cause alteration of the host rock and deposition of secondary minerals (Elders et al., 1984; Henley and Ellis, 1983). Deposition of primary minerals also occurs from high chloride deep-sourced geothermal fluids with near neutral pH, forming silica sinter on the surface (Pirajno, 2009). The circulating fluids are also detectable from surface as heat loss, through hot water bodies or steaming grounds (Hochstein and Dickinson, 1970; Seward et al., 2018).

A widely applied geophysical technique in geothermal areas is remote sensing. Remote sensing can offer reconnaissance surveys for generating maps of different hydrothermal alteration zones, minerals, thermal anomalies and geological lineaments at a faster and cheaper rate than ground-based techniques (Bedell et al., 2017; Kereszturi et al., 2020; Rathod et al., 2013). Amongst the remote sensing techniques, hyperspectral remote sensing has great value due to the number of spectral bands and their narrow bandwidth, which can be employed to characterise fine absorption features to differentiate amongst minerals (Calvin and Pace, 2016; Sabins, 1999). In combination with thermal infrared remote sensing techniques, this methodology becomes a strong tool to explore and delineate geothermal areas, particularly in non-vegetated regions (Haselwimmer et al., 2013; Romaguera et al., 2018).

However, there are many geothermal areas located in densely vegetated areas (e.g. Indonesia, Mexico, New Zealand) Densely vegetated areas can hinder optical remote sensing techniques. Even though hyperspectral and near infrared remote sensing techniques are widely employed for vegetation analysis, whereas mostly for precision agriculture (Haboudane et al., 2002; Pullanagari et al., 2017) and land remediation (Evangelides and Nobajas, 2020; Potter et al., 2012), there is big potential to harness their capability for geothermal exploration in densely vegetated settings. Geothermal areas are can be a harsh and extreme environment for vegetation, which can manifest on the vegetation cover (i.e. changes on height and decrease on species variety) (Burns, 1997; Seward et al., 2018). This study aims to identify correlations within typical vegetation indices from hyperspectral data and temperature changes in an active geothermal system.

2. GEOLOGICAL SETTING

Waiotapu Geothermal Field is located in the Taupo Volcanic Zone (TVZ), New Zealand, a region characterised by extensive rhyolitic and basaltic volcanism and associated geothermal activity (Figure 1). The high geothermal activity in this region is related to the subduction of the Pacific plate under the Australian plate, also causing normal faulting with a NE-SW orientation (Milicich et al., 2020; Wilson and Rowland, 2016). Out of the more than 20 geothermal systems within the TVZ, Waiotapu Geothermal Field is the largest by surface extension (~18 km^2) and heat flow (~500 MW).

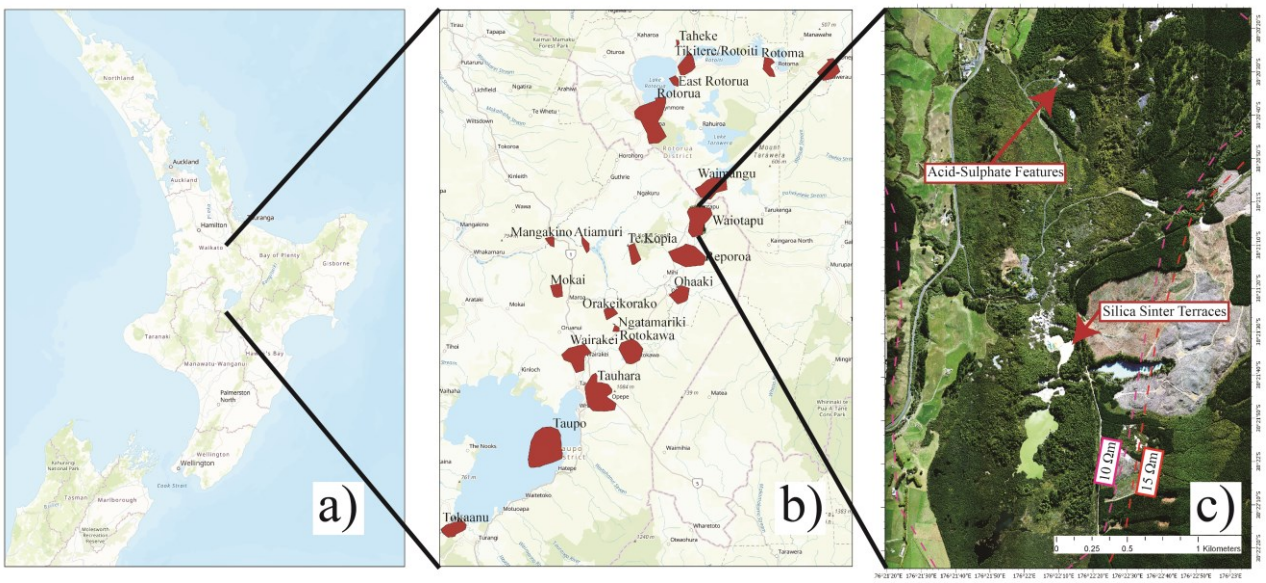

Figure 1. a) Overview map of Waiotapu Geothermal Field location within the Taupo Volcanic Zone geothermal areas of North Island of New Zealand. b) Geothermal areas in the TVZ. c) Waiotapu acquired hyperspectral image with 10 Ωm and 15 Ωm resistivity boundaries.

The TVZ basement consists of a sedimentary weakly metamorphosed rock, overlaid by extensive layers of ignimbrite and sediments (Grindley et al., 1994; Milicich et al., 2020; Steiner, 1963). Waiotapu is hosted by silicic rocks with a series of pyroclastic flows from rhyolitic eruptions (Cole, 1990; Ritchie, 1996; Wood, 1994), often interlayered with lacustrine sediments which act as a litho-cap for the hydrothermal system (Kaya et al., 2014).

Deep chloride-rich fluid heats up and rises, interacting with ground water and host rock. Developing a variety of surface features, including steaming ground, fumaroles, collapse and hydrothermal eruption craters, silica deposits and sinters, mud pools, acid-sulphate mineral alteration, hot chloride pools, sulphur-chloride and bicarbonate-chloride springs (Grange, 1937; Hedenquist and Browne, 1989; Hunt et al., 1994; Lloyd, 1959).

3. VEGETATION IN GEOTHERMAL AREAS

Vegetation in geothermal areas can be exposed to extreme conditions, including high temperatures, elevated amounts of chemical elements (i.e. As, Au, Ag, S, Hg, Sb), excess or deficiency of nutrients and water stress (Boothroyd, 2009; Burns and Leathwick, 1995; Given, 1980). Chemical in plant tissue, spectral anomalies and visible changes over time have been detected in vegetation from several geothermal systems, including the western US (Kennedy-Bowdoin et al., 2004; Martini et al., 2004; Way and Hall, 2001), southwest China (Zhou et al., 2015), Japan (Yoshii, 1937), Indonesia (Urai et al., 2000), Iceland (Elmarsdóttir et al., 2015) and New Zealand (Burns and Leathwick, 1995; Dunn, 2007; Dunn and Christie, 2019; Seward et al., 2018; Van Manen and Reeves, 2012).

The TVZ hosts most high temperature geothermal systems in New Zealand, and therefore is the main region with geothermal vegetation, where characteristic clusters of species have been identified along different geothermal fields (i.e. ferns, some moss species, manuka and kanuka). Amongst the vegetation species enduring geothermal areas, kanuka shrub (*Kunzea ericoides* var *microflora*) also referred to as prostrate kanuka, dominates in the highly active geothermal areas by being highly specialised to survive temperature and soil extremes (Van Manen and Reeves, 2012). Field surveys, multispectral remote sensing and chemical analyses, have categorised kanuka as the dominant plant species of geothermal areas in New Zealand (Beadel et al., 2018; Cochrane et al., 1994; Deroin et al., 1995; Dunn et al., 2018; Dunn and Christie, 2019; Seward et al., 2018).

Kanuka can be found in active geothermal areas in association with other tall plant species (>2 m) or with ground moss species near active geothermal features where the temperatures exceed 50 °C (Burns and Leathwick, 1995). Also, kanuka roots have been reported to associate with *pisolithus* fungi species in hot (50 °C at 8 cm depth), highly acidic and Nitrogen depleted soils (Moyersoen and Beever, 2004), these fungi facilitate the uptake of certain nutrients (Saunders, 2017). Qualitatively, plant height declines as the soil temperature increases, which is visible on the field in many geothermal areas in New Zealand (Burns and Leathwick, 1995; Cochrane et al., 1994; Given, 1980; Van Manen and Reeves, 2012).

3.1 Stress on Vegetation Detected by Remote Sensing

The stress on plants has been studied for the last 100 years (Lichtenthaler, 1996), and analysed with remote sensing approaches for the last 50 years (Birth and McVey, 1968). Remote sensing approaches have been initially focused on band ratios which compare different bands from the spectrum, usually in the visible and near infrared regions. These ratios can reflect on the vegetation health, such as chlorophyll content, quantified through the position of the red-edge around 650 - 750 nm (Dunn, 2007; Wang et al., 2018). Typically, the less chlorophyll pigment there is, the red edge shifts towards the blue part of the electromagnetic spectrum (Sanches et al., 2013; van der Meer and de Jong, 2001). The red edge shift can also indicate a change on plant health and leaf area index (Dong et al., 2019; Sellers, 1985). Vegetation indices can include Atmospherically Resistant Vegetation Index (ARVI) (Kaufman and Tanre, 1992), Normalised Difference Vegetation Index (NDVI) (Rouse et al., 1973), Red Edge NDVI (RENDVI) (Gitelson and

Merzlyak, 1994), Simple Ratio Index (SRI) (Birth and McVey, 1968), Vogelmann (VREI1) (Vogelmann et al., 1993). Other studies have evaluated water content in the Near Infrared and Short Wave Infrared regions, as canopy water content is highly relevant for vegetation health, with indices such as Moisture Stress Index (MSI) (Ceccato et al., 2001; Hunt and Rock, 1989; Vogelmann and Rock, 1986), Normalised Difference Infrared Index (NDII) (Hardisky et al., 1983; Hunt and Rock, 1989) and Water Band Index (WBI) (Champagne et al., 2001; Penuelas et al., 1993).

Remote sensing data representing the relation between vegetation indices (i.e. NDVI) and soil temperature, is typically represented in a triangular shape, with data points inside its margins (Figure 2). Variations can be related to surface soil moisture (Liu et al., 2018), slope angle (Hope and McDowell, 1992), vegetation dryness (Sandholt et al., 2002) and evapotranspiration processes (Lambin and Ehrlich, 1996).

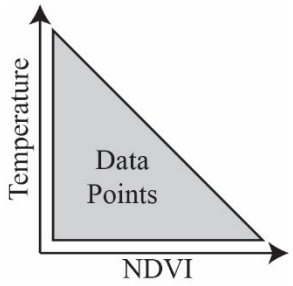

Figure 2. A simplified Temperature and NDVI data envelope from Lambina and Ehrlich (Lambin and Ehrlich, 1996).

4. DATA AND METHODS

4.1 Airborne Hyperspectral and Thermal Data Collection and Instrumentation

Hyperspectral airborne imagery acquiring data from Visible to Short Wave Infrared (VIS to SWIR) from 0.38 to 2.5 µm, was captured using an AisaFENIX push-broom, full-spectrum instrument mounted on a Cessna 185 aircraft. Collecting 448 spectral bands with a ground resolution of 1 m, detailed description on sensors can be found in Kereszturi et al., and 2018; Pullanagari et al., 2016. On 13 April 2019 (UTC +12 hrs) aerial survey was carried out in an N-S direction between 11:20 to 12:59 local time, with only 10 hours difference from the thermal infrared image acquisition flight at night.

Pre-processing of the data included radiometric correction using CaliGeoPro software package, followed by atmospheric correction using ATCOR-4 (Richter, 1998), and geo-rectification using PARGE (Schläpfer and Richter, 2002). Individual image strips were mosaicked into a full data cube. Normalised Difference Vegetation Index (NDVI) was utilized as criterion for separating vegetation in the image, with 0.4 as a threshold value. Data noise due to atmospheric interferences (1.9-2.1 µm) was removed before the image classification. Additionally, a Savitzky-Golay smoothing filter (Savitzky and Golay, 1964) was applied to the hyperspectral imagery.

On 13 of April 2019 at night between 20:30 and 23:30 the airborne Thermal infrared (TIR) image was captured, with a FLIR A615 TIR camera by GNS Science (Reeves and Sanders, 2019). Night acquisition is employed as it can minimise solar heating and solar reflection effects on the ground surface (Seward et al., 2018). Calibration includes a linear temperature calibration from water bodies measured at the time of the TIR survey, this linear equation was applied to the image to get temperature values. However, as temperatures are calibrated to water, caution is advised when examining other surface temperatures. Furthermore, vegetation will block the amount of emitted energy from soil temperatures detected by the sensor.

4.2 Image Classification

A pixel-based supervised image classification was chosen to classify vegetation cover and type using the hyperspectral image. We have chosen the Support Vector Machine (SVM) algorithm, which is a non-parametric classification algorithm based on statistical learning theory (Vapnik, 1995). It constructs a model based on the training data that is used to make predictions about the unknown data sets. A hyperplane is constructed in a high-dimensional space which best separates the labelled classes data (Gewali et al., 2018; Varshney and Arora, 2004). SVM was also chosen as it can perform well on small size training data (Mountrakis et al., 2011).

Labelled class data of vegetation types was digitized as polygons using field observation, hyperspectral imagery and high-resolution RGB photographs. From which four main types of vegetation were selected, kanuka, mixed bush, pine plantation and grass. In this study, a radial basis function kernel which is a non-linear decision boundary, was applied. Kanuka shrub represented ~35% of the image, which if combined with the ~10% of exposed soil in Waiotapu Geothermal Field (Rodriguez-Gomez et al., in review) represents a significative larger area with potential to be explored.

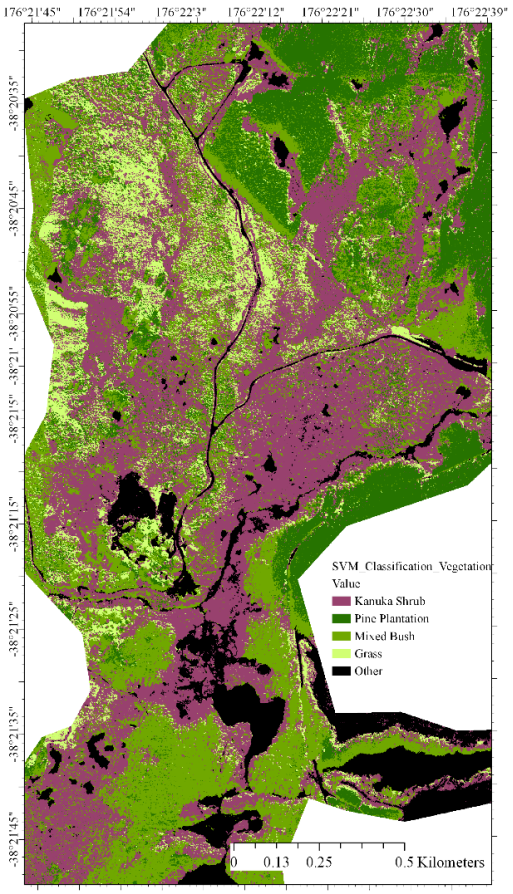

Figure 3. Image classification map using Support Vector Machine in Waiotapu Geothermal Field. This map shows the distribution of kanuka that is used to develop thermal proxies to quantify geothermal activity.

4.3 Vegetation Indices and Thermal Infrared Correlations

The areas classified as kanuka shrub were explored with 8 commonly used indices (Table 1), by extracting data from about 200 random points distributed amongst 5 temperature ranges (i.e. 0-2.5 °C, 2.5–5.5 °C, 5.5–13 °C, 13–25 °C, 25–100 °C). Buffers of 2 meters (~10 pixels) were created in each point location and averaged to reduce the noise from the image and plotted directly against the thermal infrared image data.

5. RESULTS

The SVM image classification (Figure 3) had a 98.7% overall accuracy, with kanuka shrub rarely misclassified with grass or mixed shrub. In addition to a high overall accuracy, the image classification exhibits a congruent spatial distribution of vegetation classes to what was observed on field.

Vegetation indices were visually analysed and quantitatively compared against the thermal infrared imagery (Figures 4 and 5). The 8 selected vegetation indices fitted an exponential trend with R^2 values as follows; NDVI 0.78 R^2, VREI1 0.77 R^2, RENDVI 0.76 R^2, SRI 0.73 R^2, ARI2 0.72 R^2, ARVI 0.72 R^2, WBI 0.40 R^2, and MSI 0.38 R^2.

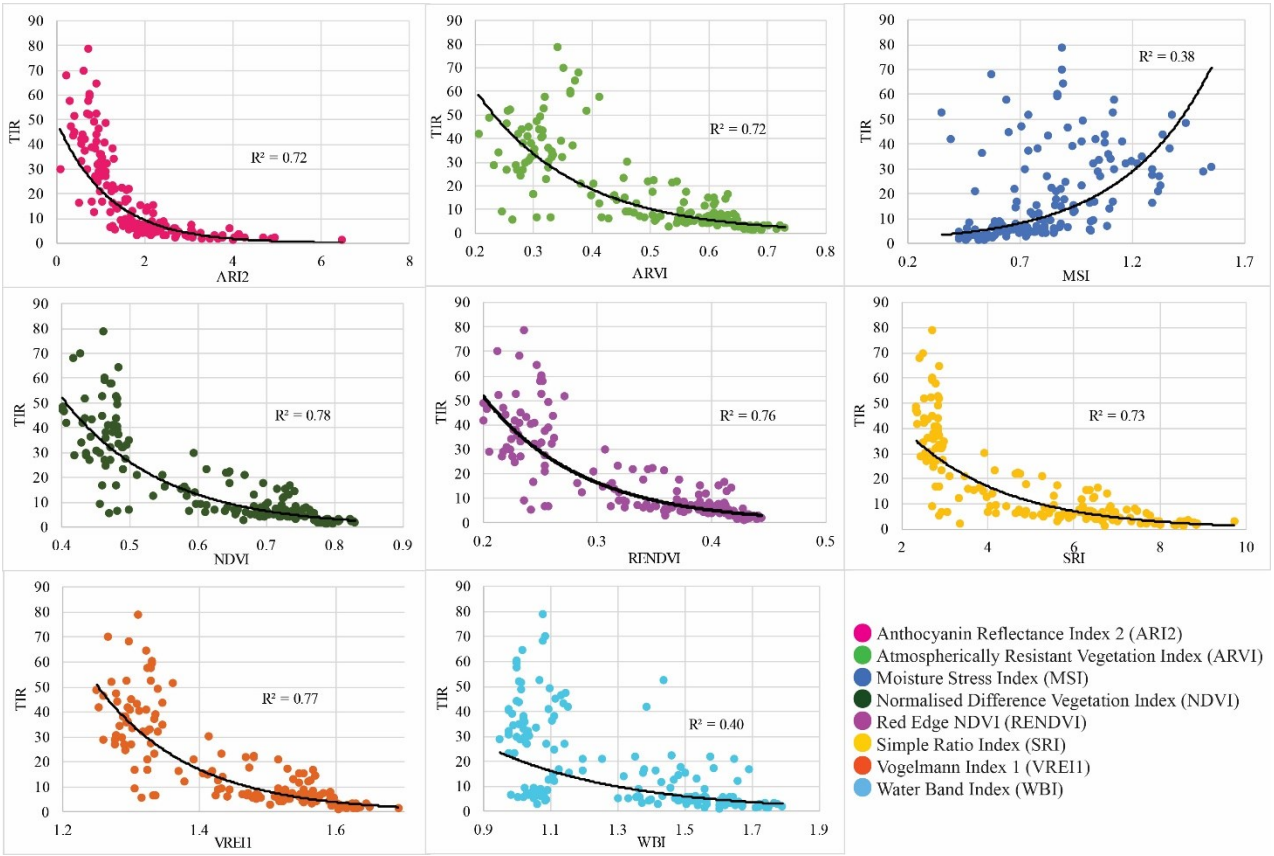

Figure 4. Vegetation Indices Plotted Against Thermal Infrared Data.

Diminishing vegetation health with increasing temperatures is an overall trend, observed throughout the 8 selected indices (Figure 4). As thermal infrared imagery was, however, calibrated against water bodies temperatures, therefore objects with different emissivity can only be used as a relative measure. Hence, as kanuka shrub has been recorded to increase height with decreasing soil temperatures, it can mask surface temperatures as a function of height. Regardless, the presented trends coincide with previous studies relating vegetation indices (i.e. NDVI) with soil temperatures (Hope and McDowell, 1992; Lambin and Ehrlich, 1996; Sandholt et al., 2002).

Some of the best fitting correlations (i.e. ARVI, NDVI, RENDVI, SRI, and VREI1) are based on red-edge values, and are directly correlated to chlorophyll concentrations (Kaufman and Tanre, 1992; Rouse et al., 1973; Slonecker et al., 2009). Chlorophyll is fundamental for photosynthetic activity, by allowing vegetation to absorb energy from light. Consequently, chlorophyll amongst other pigments are excellent indicators of overall physiological status (Elarab et al., 2015; Evans et al., 1986; Sims and Gamon, 2002). ARI2, measures anthocyanins, water soluble pigments abundant in newly forming leaves (Gamon and Surfus, 1999; Gitelson et al., 2009). Therefore, low levels in this index indicate stress on vegetation causing limited vegetation growth.

MSI and WBI plots exhibit weak correlations with temperature changes (Figure 4). These indices are based on bands from the short-wave infrared region. This region is typically noisier than the visible range for the AisaFENIX data (Pullanagari et al., 2016). The increased noise levels can interfere with an accurate reading of the canopy's water content.

Furthermore, some areas (black arrows, Figure 5-b) exhibit low values for vegetation health, while temperatures from the thermal infrared imagery are not exceedingly high (<25 °C). This could indicate stress caused by other factors than temperatures, such as limited nutrients and high concentrations of elements in the soil related to geothermal activity (i.e. As, Au, Ag, S, Hg, Sb). It could also indicate temporal activity changes, such as areas once thermally active, but cold and nutrient depleted at the present.

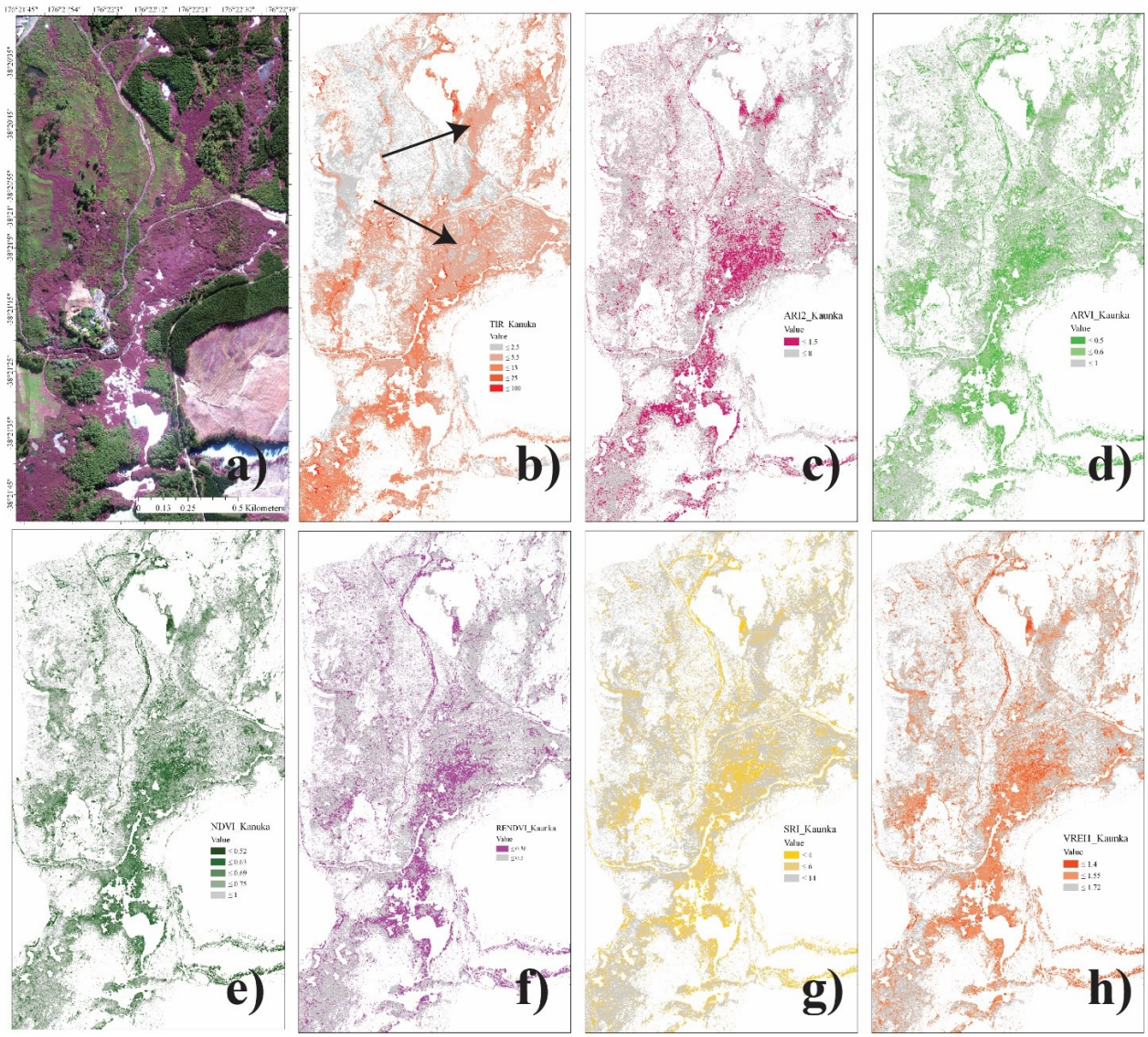

Figure 5. Map displaying the spatial distribution of kanuka, from the image classification overlain by the RGB image of the Waiotapu Geothermal Field (a), the thermal infrared imagery (b); and a series of vegetation indices: ARI2 (c), ARVI (d), NDVI (e), RENDVI (f), SRI (g), VREI1 (h).

6. CONCLUSIONS

Our study shows that simple vegetation indices from narrow band hyperspectral imagery can be used to assess the thermal stress on vegetation living around geothermal areas. This is interpreted to be due to the change of plant height (i.e. canopy structure) and health in relation to ground temperature. Vegetation indices measuring anthocyanin and chlorophyll content (NDVI, SRI, ARVI, RENDVI, VREI1 and ARI2) show good correlations with the temperatures derived from the thermal infrared imagery, at R^2 values between 0.72 and 0.78. These correlations produced the best fit with an exponential trendline, rather than a more common linear correlation. We also conclude that vegetation health living around geothermal areas is likely to get affected not only by temperature but additional stress factors.

From visual analysis, some areas may also indicate the presence of other stress factors (e.g. nutrient depletion or excess, acidic conditions, high concentration of elements (i.e. As, Au, Ag, S, Hg, Sb) or temporal changes in thermal activity). Further research should consider acquisition of LiDAR imagery to analyse vegetation height against soil temperatures. As well as, chemical concentrations, nutrient depletion and high element concentration data and their effect on geothermal vegetation spectral signature. Such analyses in combination with the presented methodology would determine how kanuka health and height relate to ground temperature, opening a new tool for geothermal exploration.

This study also illustrates the potential of utilizing vegetation as a proxy to understand subsurface geothermal at different spatial resolutions and at regional scale. For example, the calculated vegetation indices can be calculated from both broad bandwidth Sentinel-2 imagery with 10 m spatial resolution and narrow bandwidth hyperspectral PRISMA imagery acquired at 30 m spatial resolution. These satellite platforms can offer an opportunity to map vegetation proxies for geothermal activity across the whole TVZ, while it can also significantly improve our capabilities for temporal monitoring with a revisit times of 5 days and 29 days, respectively. Furthermore, this study suggests satellite thermal surrogate information now available on ~60 m spatial resolution (i.e.

ECOSTRESS) could be deduced from higher spatial resolution satellite spectral imagery, providing higher value at lower economical cost.

7. ACKNOWLEDGMENTS

We thank the Catalyst Fund for supporting this project. Massey University, School of Agriculture and Environment for the PhD scholarship and working spaces. Ngati Tahu – Ngati Whaoa Runanga Trustees and the Department of Conservation (DOC), New Zealand for sampling permits of Waiotapu Scenic Reserve.

REFERENCES

Beadel, S., Shaw, W., Bawden, R., Bycroft, C., Wilcox, F., McQueen, J., Lloyd, K., 2018. Sustainable management of geothermal vegetation in the Waikato Region, New Zealand, including application of ecological indicators and new monitoring technology trials. Geothermics 73, 91–99. https://doi.org/10.1016/j.geothermics.2017.11.001

Bedell, R.L., Rivard, B., Browning, D., Coolbaugh, M., 2017. Spectral Geology and Remote Sensing Paper 81 Thermal Infrared Sensing for Exploration and Mining-An Update on Relevant Systems for Remote Acquisition to Drill Core Scanning. Proc. Explor. 17, 881–897.

Bibby, H.M., Bennie, S.L., Stagpoole, V.M., Caldwell, T.G., 1994. Resistivity Structure of the Waimangu, Waiotapu, Waikite and Reporoa Geothermal Areas, New-Zealand. Geothermics 23, 445–471. https://doi.org/10.1016/0375-6505(94)90013-2

Birth, G.S., McVey, G.R., 1968. Measuring the Color of Growing Turf with a Reflectance Spectrophotometer 1. Agron. J. 60, 640–643. https://doi.org/10.2134/agronj1968.00021962006000060016x

Blasco, M., Gimeno, M.J., Auqué, L.F., 2018. Low temperature geothermal systems in carbonate-evaporitic rocks: Mineral equilibria assumptions and geothermometrical calculations. Insights from the Arnedillo thermal waters (Spain). Sci. Total Environ. 615, 526–539. https://doi.org/10.1016/j.scitotenv.2017.09.269

Bobos, I., Williams, L.B., 2017. Boron, lithium and nitrogen isotope geochemistry of NH4-illite clays in the fossil hydrothermal system of Harghita Bãi, East Carpathians, Romania. Chem. Geol. 473, 22–39. https://doi.org/10.1016/j.chemgeo.2017.10.005

Boothroyd, I.K.G., 2009. Ecological characteristics and management of geothermal systems of the Taupo Volcanic Zone, New Zealand. Geothermics 38, 200–209. https://doi.org/10.1016/j.geothermics.2008.12.010

Burgos, M.I.M., 1999. Geochemical interpretation of thermal fluid discharge from wells and springs in Berlin geothermal field, El Salvador. United Nations Univ. Reports 7, 165–191.

Burns, B., 1997. Vegetation change along a geothermal stress gradient at the Te Kopia steamfield. J. R. Soc. New Zeal. 27, 279–293. https://doi.org/10.1080/03014223.1997.9517539

Burns, B., Leathwick, J., 1995. Geothermal Vegetation Dynamics.

Calvin, W., Coolbaugh, M., Kratt, C., 2005. Application of remote sensing technology to geothermal exploration. Geol. Soc. Nevada Symp. 2005 Wind. to World 1083–1089. https://doi.org/10.1002/nav.3800300412

Calvin, W.M., Pace, E.L., 2016. Utilizing HyspIRI prototype data for geological exploration applications: A southern California case study. Geosci. 6. https://doi.org/10.3390/geosciences6010011

Ceccato, P., Flasse, S., Tarantola, S., Jacquemoud, S., Grégoire, J.M., 2001. Detecting vegetation leaf water content using reflectance in the optical domain. Remote Sens. Environ. 77, 22–33. https://doi.org/10.1016/S0034-4257(01)00191-2

Champagne, C., Pattey, E., Bannari, A., Stratchan, I.B., 2001. Mapping Crop Water Status: Issues of Scale in the Detection of Crop Water Stress Using Hyperspectral Indices. Proc. 8th Int. Symp. Phys. Meas. Signatures Remote Sens. 79–84.

Cochrane, G.R., Mongillo, M.A., Browne, P.R.L., Deroin, J.P., 1994. SATELLITE STUDIES OF THE WAIMANGU AND WAIOTAPU GEOTHERMAL AREAS , TVZ 181–186.

Cole, J.W., 1990. Structural control and origin of volcanism in the Taupo volcanic zone, New Zealand. Bull. Volcanol. 52, 445–459. https://doi.org/10.1007/BF00268925

Deroin, J.P., Cochrane, G.R., Mongillo, M.A., Browne, P.R., 1995. Methods of remote sensing in geothermal regions: The geodynamic setting of the Taupo Volcanic Zone (North Island, New Zealand). Int. J. Remote Sens. 16, 1663–1677. https://doi.org/10.1080/01431169508954503

Dong, T., Liu, J., Shang, J., Qian, B., Ma, B., Kovacs, J.M., Walters, D., Jiao, X., Geng, X., Shi, Y., 2019. Assessment of red-edge vegetation indices for crop leaf area index estimation. Remote Sens. Environ. 222, 133–143. https://doi.org/10.1016/j.rse.2018.12.032

Dunn, C.E., 2007. Biogeochemistry in Mineral Exploration.

Dunn, C.E., Black, J., Christie, A.B., 2018. Biogeochemical Surveys at Ohui and Pine Sinter Epithermal Au-Ag Prospects , Coromandel , and at Waiotapu Thermal Park , New Zealand J Black , GNS Science , PO Box 30368 , Lower Hutt 5040 , New Zealand. https://doi.org/10.21420/G25647.CE

Dunn, C.E., Christie, A.B., 2019. Tree ferns and tea trees in biogeochemical exploration for epithermal Au and Ag in New Zealand. Geochemistry Explor. Environ. Anal. geochem2019-047. https://doi.org/10.1144/geochem2019-047

Elarab, M., Ticlavilca, A.M., Torres-Rua, A.F., Maslova, I., McKee, M., 2015. Estimating chlorophyll with thermal and broadband

multispectral high resolution imagery from an unmanned aerial system using relevance vector machines for precision agriculture. Int. J. Appl. Earth Obs. Geoinf. 43, 32–42. https://doi.org/10.1016/j.jag.2015.03.017

Elders, W.A., Bird, D.K., Williams, A.E., Schiffman, P., 1984. Hydrothermal flow regime and magmatic heat source of the Cerro Prieto geothermal system, Baja California, Mexico. Geothermics 13, 27–47. https://doi.org/10.1016/0375-6505(84)90005-1

Elmarsdóttir, Á., Vilmundardóttir, O.K., Magnússon, S.H., 2015. Vegetation of High-temperature Geothermal Areas in Iceland 19–25.

Evangelides, C., Nobajas, A., 2020. Red-Edge Normalised Difference Vegetation Index (NDVI705) from Sentinel-2 imagery to assess post-fire regeneration. Remote Sens. Appl. Soc. Environ. 17, 100283. https://doi.org/10.1016/j.rsase.2019.100283

Evans, D.L., Farr, T.G., Ford, J.P., Thompson, T.W., Werner, C.L., 1986. Multipolarization Radar Images for Geologic Mapping and Vegetation Discrimination. IEEE Trans. Geosci. Remote Sens. GE-24, 246–257. https://doi.org/10.1109/TGRS.1986.289644

Gamon, J.A., Surfus, J.S., 1999. Assessing leaf pigment content and activity with a reflectometer. New Phytol. 143, 105–117. https://doi.org/10.1046/j.1469-8137.1999.00424.x

Gewali, U.B., Monteiro, S.T., Saber, E., 2018. Machine learning based hyperspectral image analysis: A survey.

Gitelson, A., Merzlyak, M.N., 1994. Spectral Reflectance Changes Associated with Autumn Senescence of Aesculus hippocastanum L. and Acer platanoides L. Leaves. Spectral Features and Relation to Chlorophyll Estimation. J. Plant Physiol. 143, 286–292. https://doi.org/10.1016/S0176-1617(11)81633-0

Gitelson, A.A., Chivkunova, O.B., Merzlyak, M.N., 2009. Nondestructive estimation of anthocyanins and chlorophylls in anthocyanic leaves. Am. J. Bot. 96, 1861–1868. https://doi.org/10.3732/ajb.0800395

Given, D.R., 1980. Vegetation on heated soils at Karapiti, Central North Island, New Zealand, And its relation to ground. New Zeal. J. Bot. 18, 1–13. https://doi.org/10.1080/0028825X.1980.10427227

Grange, L., 1937. The Geology of the Rotorua-Taupo Subdivision, Rotorua and Kaimanawa Divisions. New Zeal. Dep. Sci. Ind. Res. Bull. 37, 86–105.

Grindley, G., Mumme, T., Kohn, B., 1994. Stratigraphy, paleomagnetism, geochronology and structure of silicic volcanic rocks, Waiotapu/Paeroa range area, New Zealand. Geothermics 23, 473–499. https://doi.org/10.1016/0375-6505(94)90014-0

Haboudane, D., Miller, J.R., Tremblay, N., Zarco-Tejada, P.J., Dextraze, L., 2002. Integrated narrow-band vegetation indices for prediction of crop chlorophyll content for application to precision agriculture. Remote Sens. Environ. 81, 416–426. https://doi.org/10.1016/S0034-4257(02)00018-4

Hardisky, M.A., Klemas, V., Smart, R.M., 1983. The influence of soil salinity, growth form, and leaf moisture on the spectral radiance of Spartina alterniflora canopies. Photogramm. Eng. Remote Sens. 49, 77–83.

Haselwimmer, C., Prakash, A., Holdmann, G., 2013. Quantifying the heat flux and outflow rate of hot springs using airborne thermal imagery: Case study from Pilgrim Hot Springs, Alaska. Remote Sens. Environ. 136, 37–46. https://doi.org/10.1016/j.rse.2013.04.008

Hedenquist, J.W., Browne, P.R.L., 1989. The evolution of the Waiotapu geothermal system, New Zealand, based on the chemical and isotopic composition of its fluids, minerals and rocks. Geochim. Cosmochim. Acta 53, 2235–2257. https://doi.org/10.1016/0016-7037(89)90347-5

Henley, R.W., Ellis, A.J., 1983. Geothermal systems ancient and modern: a geochemical review. Earth Sci. Rev. 19, 1–50. https://doi.org/10.1016/0012-8252(83)90075-2

Hochstein, M.P., Dickinson, D.J., 1970. Infra-red remote sensing of thermal ground in the Taupo region, New Zealand. Geothermics 2. https://doi.org/10.1016/0375-6505(70)90039-8

Hochstein, M.P., Soengkono, S., 1997. Magnetic anomalies associated with high temperature reservoirs in the Taupo volcanic zone (New Zealand). Geothermics 26, 1–24. https://doi.org/10.1016/S0375-6505(96)00028-4

Hope, A.S., McDowell, T.P., 1992. The relationship between surface temperature and a spectral vegetation index of a tallgrass prairie: Effects of burning and other landscape controls. Int. J. Remote Sens. 13, 2849–2863. https://doi.org/10.1080/01431169208904086

Hunt, E.R., Rock, B.N., 1989. Detection of changes in leaf water content using Near- and Middle-Infrared reflectances. Remote Sens. Environ. 30, 43–54. https://doi.org/10.1016/0034-4257(89)90046-1

Hunt, T.M., Glover, R.B., Wood, C.P., 1994. Waimangu, Waiotapu, and Waikite Geothermal Systems, New Zealand: Backgound History. Geothermics 23, 379–400.

Kaufman, Y.J., Tanre, D., 1992. Atmospherically resistant vegetation index (ARVI) for EOS-MODIS. IEEE Trans. Geosci. Remote Sens. 30, 261–270. https://doi.org/10.1109/36.134076

Kaya, E., O'Sullivan, M.J., Hochstein, M.P., 2014. A three dimensional numerical model of the Waiotapu, Waikite and Reporoa geothermal areas, New Zealand. J. Volcanol. Geotherm. Res. 283, 127–142. https://doi.org/10.1016/j.jvolgeores.2014.07.008

Kennedy-Bowdoin, T., Silver, E.A., Martini, B.A., Pickles, W.L., 2004. Geothermal prospecting using hyperspectral imaging and field observations, Dixie Meadows, NV. Geotherm. Resour. Counc. Trans. 28, 19–22.

Kereszturi, G., Schaefer, L.N., Miller, C., Mead, S., 2020. Hydrothermal Alteration on Composite Volcanoes: Mineralogy, Hyperspectral Imaging, and Aeromagnetic Study of Mt Ruapehu, New Zealand. Geochemistry, Geophys. Geosystems 21, 1–28. https://doi.org/10.1029/2020gc009270

Kereszturi, G., Schaefer, L.N., Schleiffarth, W.K., Procter, J., Pullanagari, R.R., Mead, S., Kennedy, B., 2018. Integrating airborne hyperspectral imagery and LiDAR for volcano mapping and monitoring through image classification. Int. J. Appl. Earth Obs. Geoinf. 73, 323–339. https://doi.org/10.1016/j.jag.2018.07.006

Lambin, E.F., Ehrlich, D., 1996. The surface temperature-vegetation index space for land cover and land-cover change analysis. Int. J. Remote Sens. 17, 463–487. https://doi.org/10.1080/01431169608949021

Lichtenthaler, H.K., 1996. Vegetation Stress: an Introduction to the Stress Concept in Plants. J. Plant Physiol. 148, 4–14. https://doi.org/10.1016/s0176-1617(96)80287-2

Liu, Z., Yao, Z., Wang, R., 2018. Evaluating the surface temperature and vegetation index (Ts/VI) method for estimating surface soil moisture in heterogeneous regions. Hydrol. Res. 49, 689–699. https://doi.org/10.2166/nh.2017.079

Lloyd, E.F., 1959. The Hot Springs and Hydrothermal Eruptions of Waiotapu. New Zeal. J. Geol. Geophys. 2, 141–176. https://doi.org/10.1080/00288306.1959.10431319

Martini, B.A., Cocks, T.D., Cocks, P.A., Hausknecht, P., Pickles, W.L., 2004. Operational airborne hyperspectral remote sensing for global geothermal exploration. Int. Geosci. Remote Sens. Symp. 1, 625–626. https://doi.org/10.1109/igarss.2004.1369105

Mauriohooho, K., Barker, S.L.L., Rae, A.J., Simpson, M.P., 2014. Hydrothermal Alteration of the Tauhara Geothermal Field, an active hydrothermal system. AusIMM New Zeal. Branch Annu. Conf. 2014 371–381.

Milicich, S.D., Mortimer, N., Villamor, P., Wilson, C.J.N., Sagar, M.W., Ireland, T.R., Milicich, S.D., Mortimer, N., Villamor, P., Wilson, C.J.N., Chambefort, I., Sagar, M.W., Ireland, T.R., Mesozoic, T., 2020. The Mesozoic terrane boundary beneath the Taupo Volcanic Zone , New Zealand , and potential controls on geothermal system characteristics The Mesozoic terrane boundary beneath the Taupo Volcanic Zone , New. New Zeal. J. Geol. Geophys. 0, 1–12. https://doi.org/10.1080/00288306.2020.1823434

Mongillo, M.A., 1994. Aerial Thermal Infrared Mapping of the Waimangu-Waiotapu Geothermal Region, New Zealand. Geothermics 23, 379–400.

Mountrakis, G., Im, J., Ogole, C., 2011. Support vector machines in remote sensing: A review. ISPRS J. Photogramm. Remote Sens. 66, 247–259. https://doi.org/10.1016/j.isprsjprs.2010.11.001

Moyersoen, B., Beever, R.E., 2004. Abundance and characteristics of Pisolithus ectomycorrhizas in New Zealand geothermal areas. Mycologia 96, 1225–1232. https://doi.org/10.1080/15572536.2005.11832871

Penuelas, J., Filella, I., Biel, C., Serrano, L., Save, R., 1993. The reflectance at the 950-970 nm region as an indicator of plant water status. Int. J. Remote Sens. 14, 1887–1905. https://doi.org/10.1080/01431169308954010

Pirajno, F., 2009. Hydrothermal Processes and Mineral Systems, Journal of Chemical Information and Modeling.

Potter, C., Li, S., Huang, S., Crabtree, R.L., 2012. Analysis of sapling density regeneration in Yellowstone National Park with hyperspectral remote sensing data. Remote Sens. Environ. 121, 61–68. https://doi.org/10.1016/j.rse.2012.01.019

Pullanagari, R.R., Kereszturi, G., Yule, I.J., 2017. Quantification of dead vegetation fraction in mixed pastures using AisaFENIX imaging spectroscopy data. Int. J. Appl. Earth Obs. Geoinf. 58, 26–35. https://doi.org/10.1016/j.jag.2017.01.004

Pullanagari, R.R., Kereszturi, G., Yule, I.J., 2016. Mapping of macro and micro nutrients of mixed pastures using airborne AisaFENIX hyperspectral imagery. ISPRS J. Photogramm. Remote Sens. 117, 1–10. https://doi.org/10.1016/j.isprsjprs.2016.03.010

Rathod, P.H., Rossiter, D.G., Noomen, M.F., van der Meer, F.D., 2013. Proximal Spectral Sensing to Monitor Phytoremediation of Metal-Contaminated Soils. Int. J. Phytoremediation 15, 405–426. https://doi.org/10.1080/15226514.2012.702805

Reeves, R., Rae, L., 2016. Changes in aerial thermal infrared signature over the Rotorua Geothermal Field, New Zealand: 1990–2014. Geothermics 64, 262–270. https://doi.org/10.1016/j.geothermics.2016.06.007

Reeves, R., Sanders, F., 2019. 2019 Thermal infrared survey of the Waiotapu Geothermal Field. https://doi.org/10.21420/ZD6D-GD88.

Richter, R., 1998. Correction of satellite imagery over mountainous terrain. Appl. Opt. 37, 4004. https://doi.org/10.1364/AO.37.004004

Ritchie, A.B.H., 1996. Volcanic Geology and Geochemistry of Waiotapu Ignimbrite, Taupo Volcanic Zone, New Zealand.

Rodriguez-Gomez, C., Kereszturi, G., Reeves, R., Rae, A., Pullanagari, R., Jeyakumar, P., Procter, J.N., n.d. Characterisation of surface alteration types on partially vegetated geothermal systems using hyperspectral and thermal remote sensing and ground exploration techniques.

Romaguera, M., Vaughan, R.G., Ettema, J., Izquierdo-Verdiguier, E., Hecker, C.A., van der Meer, F.D., 2018. Detecting geothermal anomalies and evaluating LST geothermal component by combining thermal remote sensing time series and land surface model data. Remote Sens. Environ. 204, 534–552. https://doi.org/10.1016/j.rse.2017.10.003

Rouse, J.W., Hass, R.H., Schell, J.A., Deering, D.W., 1973. Monitoring vegetation systems in the great plains with ERTS. Third

Earth Resour. Technol. Satell. Symp. 1, 309–317. https://doi.org/citeulike-article-id:12009708

Sabins, F.F., 1999. Remote Sensing for Mineral Exploration. Ore Geol. Rev. 14, 157–183.

Sanches, I.D., Souza Filho, C.R., Magalhães, L.A., Quitério, G.C.M., Alves, M.N., Oliveira, W.J., 2013. Unravelling remote sensing signatures of plants contaminated with gasoline and diesel: An approach using the red edge spectral feature. Environ. Pollut. 174, 16–27. https://doi.org/10.1016/j.envpol.2012.10.029

Sandholt, I., Rasmussen, K., Andersen, J., 2002. A simple interpretation of the surface temperature/vegetation index space for assessment of surface moisture status. Remote Sens. Environ. 79, 213–224. https://doi.org/10.1016/S0034-4257(01)00274-7

Saunders, L., 2017. The Mānuka and Kānuka Plantation Guide.

Savitzky, A., Golay, M.J.E., 1964. Smoothing and Differentiation of Data by Simplified Least Squares Procedures. Anal. Chem. 36, 1627–1639. https://doi.org/10.1021/ac60214a047

Schläpfer, D., Richter, R., 2002. Geo-atmospheric processing of airborne imaging spectrometry data. Part 1: Parametric orthorectification. Int. J. Remote Sens. 23, 2609–2630. https://doi.org/10.1080/01431160110115825

Sellers, P.J., 1985. Canopy reflectance, photosynthesis and transpiration. Int. J. Remote Sens. 6, 1335–1372. https://doi.org/10.1080/01431168508948283

Seward, A., Ashraf, S., Reeves, R., Bromley, C., 2018. Improved environmental monitoring of surface geothermal features through comparisons of thermal infrared, satellite remote sensing and terrestrial calorimetry. Geothermics 73, 60–73. https://doi.org/10.1016/j.geothermics.2018.01.007

Simpson, M.P., Rae, A.J., 2018. Short-wave infrared (SWIR) reflectance spectrometric characterisation of clays from geothermal systems of the Taupō Volcanic Zone, New Zealand. Geothermics 73, 74–90. https://doi.org/10.1016/j.geothermics.2018.01.006

Sims, D.A., Gamon, J.A., 2002. Relationships between leaf pigment content and spectral reflectance across a wide range of species, leaf structures and developmental stages. Remote Sens. Environ. 81, 337–354. https://doi.org/10.1016/S0034-4257(02)00010-X

Slonecker, T., Haack, B., Price, S., 2009. Spectroscopic analysis of arsenic uptake in Pteris ferns. Remote Sens. 1, 644–675. https://doi.org/10.3390/rs1040644

Steiner, A., 1963. The rocks penetrated by drillholes in the Waiotapu thermal area, and their hydrothermal alteration. In Waiotapu Geothermal Field. New Zeal. Dep. Sci. Ind. Res. Bull. 155, 26–35.

Urai, M., Muraoka, H., Nasution, A., 2000. Remote Sensing Study for Geothermal Development in the Ngada District , Cntral Flores , Indonesia. Proc. World Geotherm. Congr. 2000 1, 1905–1908.

van der Meer, F., de Jong, S.M., 2001. Imaging Spectrometry. Dordrecht, Netherlands.

Van Manen, S.M., Reeves, R., 2012. An assessment of changes in kunzea ericoides var. microflora and other hydrothermal vegetation at the Wairakei-Tauhara geothermal field, New Zealand. Environ. Manage. 50, 766–786. https://doi.org/10.1007/s00267-012-9899-1

Vapnik, V.N., 1995. The Nature of Statistical Learning Theory, First. ed.

Varshney, P., Arora, M., 2004. Image Processing Techniques for Remotely Sensed Hyperspectral Data.

Vogelmann, J.E., Rock, B.N., 1986. Assessing forest decline in coniferous forests of Vermont using NS-001 Thematic Mapper Simulator data. Int. J. Remote Sens. 7, 1303–1321. https://doi.org/10.1080/01431168608948932

Vogelmann, J.E., Rock, B.N., Moss, D.M., 1993. Red edge spectral measurements from sugar maple leaves. Int. J. Remote Sens. 14, 1563–1575. https://doi.org/10.1080/01431169308953986

Wang, F., Gao, J., Zha, Y., 2018. Hyperspectral sensing of heavy metals in soil and vegetation: Feasibility and challenges. ISPRS - J. Photogramm. Remote Sens. 136, 73–84.

Way, W., Hall, S., 2001. Cost-effective vegetation anomaly mapping for geotherma exploration. Proc. Twenty-Sixth Work. Geotherm. Reserv. Eng. Stanford Univ. Stanford, California, January 29-30, 2001 SGP-TR-168 2.

Wilson, C.J.N., Houghton, B.F., McWilliams, M.O., Lanphere, M.A., Weaver, S.D., Briggs, R.M., 1995. Volcanic and structural evolution of Taupo Volcanic Zone, New Zealand: a review. J. Volcanol. Geotherm. Res. 68, 1–28. https://doi.org/10.1016/0377-0273(95)00006-G

Wilson, C.J.N., Rowland, J. V., 2016. The volcanic, magmatic and tectonic setting of the Taupo Volcanic Zone, New Zealand, reviewed from a geothermal perspective. Geothermics 59, 168–187. https://doi.org/10.1016/j.geothermics.2015.06.013

Wood, C.P., 1994. Aspects of the geology of Waimangu, Waiotapu, Waikite and Reporoa geothermal systems, Taupo Volcanic Zone, New Zealand. Geothermics 23, 401–421. https://doi.org/10.1016/0375-6505(94)90011-6

Yoshii, Y., 1937. Aluminium Requirements of Solfatara-plants. Shokubutsugaku Zasshi 51, 262–270. https://doi.org/10.15281/jplantres1887.51.262

Zhou, W.N., White, J.F., Soares, M.A., Torres, M.S., Zhou, Z.P., Li, H.Y., 2015. Diversity of fungi associated with plants growing in geothermal ecosystems and evaluation of their capacities to enhance thermotolerance of host plants. J. Plant Interact. 10, 305–314. https://doi.org/10.1080/17429145.2015.1101495